Image Splicing Localization Based on Blur Type Inconsistency

Khosro Bahrami and Alex C. Kot
Rapid-Rich Object Search Lab, School of Electrical and Electronic Engineering
Nanyang Technological University, Singapore 639798

***Abstract*—In a spliced blurred image, the spliced region and the original image may have different blur types. Splicing localization in this image is challenging when a forger uses image resizing as anti-forensics to remove the splicing traces anomalies. In this paper, we overcome this problem by proposing a method for splicing localization based on partial blur type inconsistency. In this method, after the block-based image partitioning, a local blur type detection feature is extracted from the estimated local blur kernels. The image blocks are classified into out-of-focus or motion blur based on this feature to generate invariant blur type regions. Finally a fine splicing localization is applied to increase the precision of regions boundary. We can use the blur type differences of the regions to trace the inconsistency for the splicing localization. Our experimental results show the efficiency of the proposed method in the detection and the classification of the out-of-focus and motion blur types.**

I. Introduction and Background

Using the professional photo-editing tools, image tampering can be performed easily. Since images can be used in journalism, police investigation and as court evidences, image tampering can be a threat to the security of people and our society. Image splicing is one of the most common types of image tampering. In splicing of the blurred images, if the original image and the spliced region have different blur types, e.g., out-of-focus and motion, an inconsistency in the blur types of different regions may appear in the tampered image.

We focus on the detection of such kind of inconsistency for splicing localization in a blurred image. However, the forger may remove the anomaly introduced by the traces of splicing and make the image visually pleasant by resizing the tampered image into a smaller size. Such operation removes the artifacts used by many existing techniques to make the detection of splicing difficult. In this paper, we address this problem by targeting the partial blur type inconsistency detection which is almost robust to with after image resizing.

Fig.1 (a) shows an authentic image with out-of-focus blur and (b) a spliced image generated by splicing a motion blurred region in image (a). The spliced region with motion blur indicates the camera movement with respect to the scene while the original image has the out-of-focus blur. Since the objects in these regions are stationary, such inconsistency in the blur types can be used for splicing localization. In this paper, the objective is the localization of the spliced region in a tampered blurred image by exploration the inconsistency in the partial blur types.

The existing techniques of splicing localization in a tampered image [1] can be categorized into (1) format-based such as DJPG compression detection [2]; (2) camera-based such as demosaicing regularity [3]-[4], camera response function [5] and sensor pattern noise [6]; (3) pixel-based such as resampling [7], contrast enhancement detection [8] and blur degree inconsistency [9]; (4) physically-based such as light anomalies [10] and size inconsistencies [11]. These techniques have some limitations in splicing localization in a tampered blurred image when resizing is applied after splicing.

(a) Authentic image (b) Spliced image

Fig. 1: (a) An authentic image with out-of-focus blur, (b) A spliced image generated by splicing a motion blurred region in image (a), which has inconsistent blur types in the bottom (motion blur) and top (out-of-focus blur).

Some works have been done for partial blur type detection and classification. For example, Chen *et al.* [12] proposed a method based on the lowest directional high-frequency energy to classify motion and out-of-focus blurs. Liu *et al.* [13] used the correlation of shifted blocks as a feature for motion and out-of-focus blurs classification. Su *et al.* [14] proposed a method for the segmentation of motion and out-of-focus blurred regions in the partial blurred images based on alpha channel feature. Aizenberg *et al.* [15] proposed a method for segmentation of motion, gaussian and uniform blurs based on the magnitude of cepstrum coefficients. However, for partial blur type detection, these methods have low performance. In our previous work [16], we proposed a method for splicing detection based on blur type inconsistency. However, different from it, this work has been proposed for splicing localization.

The rest of this paper is organized as follows. In section II, we propose a partial blur type detection and classification method used for splicing localization in blurred images. Experimental results are shown in section III. Section IV concludes the paper.

II. Proposed Method

The proposed method for splicing localization is explained in the following sections.

978-1-4799-8391-9/15/$31.00 ©2015 IEEE

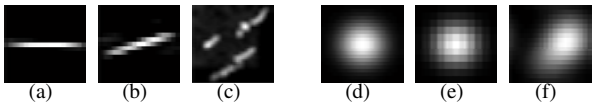

Fig. 2: Examples of blur kernels: (a)-(c) motion blur kernels, (d)-(f) out-of-focus blur kernels.

A. Blur Type Feature Extraction

Given a color image $\mathbf{B}$ of size $M \times N$, we convert into a gray scale image $\mathbf{G}$ and then partition $\mathbf{G}$ into blocks $\mathbf{G}_{i,j}$ with $L \times L$ pixels, where i and j are the index for different blocks ($1 \leq i \leq \lfloor \frac{M}{L} \rfloor$, $1 \leq j \leq \lfloor \frac{N}{L} \rfloor$). For an image block $\mathbf{G}_{i,j}$, the image blurring process is given by

$$\mathbf{G}_{i,j} = \mathbf{I}_{i,j} * \mathbf{K}_{i,j} + \mathbf{N}_{i,j} \tag{1}$$

where $\mathbf{I}_{i,j}$ represents a sharp image block, $\mathbf{K}_{i,j}$ is a local blur kernel represented by a two-dimensional matrix with size of $\kappa \times \kappa$, $\mathbf{N}_{i,j}$ is the noise matrix and '$*$' denotes convolution. To estimate $\mathbf{K}_{i,j}$ from $\mathbf{G}_{i,j}$, we use [18] which is independent of the blur type and applicable for small patches to estimate all local blur kernels $\mathbf{K}_{i,j}$ of the image $\mathbf{G}$.

Fig. 2 shows the top view of some blur kernel examples with brighter regions indicating larger values. We observe that despite of the kernel size, motion blur kernels tend to be sparse because most values in these kernels are close to zero (dark regions) while out-of-focus blur kernels are less sparse. We use such differences to extract a set of features by describing the blur kernel distributions roughly with Generalized Gaussian Distribution (GGD) below.

$$f(\mathbf{K}; \mu, \gamma, \sigma) = \left(\frac{\gamma}{2\sigma\Gamma(\frac{1}{\gamma})\sqrt{\frac{\Gamma(\frac{1}{\gamma})}{\Gamma(\frac{3}{\gamma})}}} \right) e^{-\left(\frac{\mathbf{K}-\mu}{\sigma\sqrt{\frac{\Gamma(\frac{1}{\gamma})}{\Gamma(\frac{3}{\gamma})}}} \right)^{\gamma}} \tag{2}$$

where $\mathbf{K}$ is the blur kernel estimated from a given region, $\Gamma(.)$ is the gamma function, μ is the mean, σ is the standard deviation and γ ($\gamma > 0$) is the shape-parameter of the GGD. Due to the difference in the distributions of the out-of-focus and motion blur kernels, the values of γ and σ suggest distinctive difference in values. To explore such differences, we plot in Fig. 3 the 2D scatter plot of γ versus σ for the blur kernels estimated from a set of randomly selected 800 (400 out-of-focus and 400 motion) blurred images. The value of γ in the out-of-focus blur kernels is larger than the motion blur kernels, while σ in the out-of-focus blur kernels is smaller than motion blur kernels. Such scatter plot shows that these two classes of kernels from motion and out-of-focus can easily be separable.

Based on such differences, γ and σ can be used as features for blur type classification. We propose these features for local blur type detection by describing the local blur kernels $\mathbf{K}_{i,j}$ with GGD by replacing $\mathbf{K}$ with $\mathbf{K}_{i,j}$ in Eq. (2). As such, the shape-parameter $\gamma_{i,j}$ and standard deviation $\sigma_{i,j}$, representing blur type features at block level, are used in the next section for blur type classification.

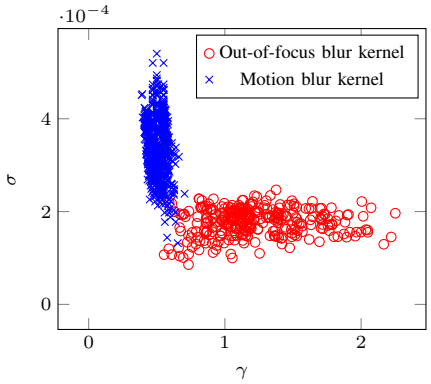

Fig. 3: 2D scatter plot of γ vs σ for Generalized Gaussian Distribution of the blur kernels estimated from 400 out-of-focus and 400 motion blurred images.

B. Blur Type Classification

In this section, we incorporate the proposed blur type features to classify the blur type of image block $G_{i,j}$ into out-of-focus or motion. We generate a new feature $\nu_{i,j}$ by combining $\gamma_{i,j}$ and $\sigma_{i,j}$ for dimensionality reduction. By representing $\gamma_{i,j}$ and $\sigma_{i,j}$ as the feature vector $\mathbf{x}_{i,j} = [\gamma_{i,j}\ \sigma_{i,j}]^T$, we define a mapping $\nu_{i,j} = f(\mathbf{x}_{i,j})$. In general, the optimal mapping $\nu_{i,j} = f(\mathbf{x}_{i,j})$ is a non-linear function. Since there is no systematic way to generate non-linear transform, we reduce the dimensionality based on linear transform of LDA [19], to yield

$$\nu_{i,j} = \mathbf{w}^T \mathbf{x}_{i,j} = [w_\gamma\ w_\sigma][\gamma_{i,j}\ \sigma_{i,j}]^T \tag{3}$$

where $\mathbf{w} = [w_\gamma\ w_\sigma]^T$ is the vector which projects the γ- and σ-axis onto a line. To find the best projection, the Fisher linear discriminant [19] suggests maximizing between-class scatter and minimizing the within-class scatter. Applying this rule for two classes of out-of-focus and motion blurs, yields

$$\mathbf{w} = {\mathbf{S}_w}^{-1}(\mathbf{e}_O - \mathbf{e}_M) \tag{4}$$

where $\mathbf{e}_O = [e_{\gamma O}\ e_{\sigma O}]^T$ and $\mathbf{e}_M = [e_{\gamma M}\ e_{\sigma M}]^T$ are the vectors of the mean of $\gamma_{i,j}$ and $\sigma_{i,j}$ in out-of-focus and motion blur classes, respectively, and $\mathbf{S}_w$ is the within-class scatter matrix obtained from

$$\mathbf{S}_w = \mathbf{S}_O + \mathbf{S}_M \tag{5}$$

where $\mathbf{S}_O$ and $\mathbf{S}_M$ are the variances of $\gamma_{i,j}$ and $\sigma_{i,j}$ in out-of-focus and motion blur classes, respectively. Using the generated feature, $\nu_{i,j}$, we formulate a binary classifier to classify the blur type of the image block $\mathbf{G}_{i,j}$, denoted as $B_{i,j}$, as out-of-focus or motion, where

$$B_{i,j} = \begin{cases} \text{'M' (motion blur)}, & \text{if } \nu_{i,j} \geq \rho \\ \text{'O' (out-of-focus blur)}, & \text{otherwise} \end{cases} \tag{6}$$

and ρ is the threshold that discriminates the blur type of an image block into out-of-focus or motion.

By defining two classes including out-of-focus blur as the positive class and motion blur as the negative class, the true positive rate (TPR) and true negative rate (TNR) are the detection accuracy of out-of-focus blur and motion blur regions, respectively. The threshold ρ is chosen in such a way to maximize the average of TPR and TNR on a training set of images. Also, to calculate the projection vector $\mathbf{w}$, we use the

training set of out-of-focus and motion blurred images. Using the calculated ρ and $\mathbf{w}$, we measure the performance for the testing set.

Since the blocks without content (smooth blocks) are not reliable in blur type detection, the image blocks are categorized into smooth and non-smooth using the method in [20]. After the blur type classification, a refinement is applied to classify the smooth blocks based on the blur type of the nearest non-smooth ones. If a smooth block has more than one nearest non-smooth block with different blur types, the majority of blur types indicates the blur type of the smooth block. Such a classification discriminates the image into s regions $R_1, R_2, ..., R_s$, where s may change from 2 to $\lfloor \frac{M}{L} \rfloor \times \lfloor \frac{N}{L} \rfloor$ (the number of image blocks).

C. Splicing Localization

After the generation of s regions $R_1, R_2, ..., R_s$, we increase the boundary precision of the regions to pixel level. First, we define boundary blocks as the ones which at least one of their 4-neighbors are from a different region. Second, we assign the labels '1', '2', ..., 's' to the pixels of all non-boundary blocks in the regions $R_1, R_2, ..., R_s$, respectively. The remaining pixels of the boundary blocks are non-labeled.

Third, we apply an energy-based technique [21] to propagate the labels from labeled pixels to non-labeled pixels by interpolation. Using the matting Laplacian, the interpolation problem can be formulated by minimizing a cost function. This cost function considers pixels intensity in addition to the labels to discriminate the pixels based on the different intensities. Since it is likely that the intensity of the pixels around the boundary of the spliced region and the original image are different, by considering the pixels intensity, a fine boundary localization can be achieved. After assigning the labels to all pixels of the boundary blocks, we generate the regions $R'_1, R'_2, ..., R'_s$ from the corresponding pixels.

After generation of $R'_1, R'_2, ..., R'_s$, a human decision is needed to indicate the spliced region based on the some inconsistencies between the blur type and semantic of the image. Such inconsistencies can be discovered based on the following facts to detect possible forgery: (1) In an image with out-of-focus blur, the stationary objects, e.g. building, should not have motion blur. (2) In an image with hand shaking or camera motion blur, all the objects should have motion blur, unless the object is stationary with respect to the camera. In such a case, the spliced region and the original image are differentiated by the blur type regions.

III. Experimental Results

In this section, firstly we evaluate the performance of the proposed method for splicing localization by comparing with some of the state-of-the-art methods in partial blur type detection, including Chen *et al.* [12], Su *et al.* [14] and Aizenberg *et al.* [15]. We took 800 natural blurred photos (400 out-of-focus and 400 motion) in TIFF noncompressed format with size of ranging from 1024×768 to 3456×2304 pixels, from 4 cameras. The ground truth of motion vs out-of-focus blurs being recorded properly. To generate the motion blurred images, we create motion with the camera in various degrees when taking pictures. To generate the out-of-focus blurred images, we took the blurred photos by using the manual focusing in various degrees. When taking the out-of-focus blurred photos, the camera was mounted onto the tripod stand to ensure maximum stability so that the cause of the natural blur was only due to the manual focusing controlled by the user.

TABLE I: Performance comparison of the methods for splicing localization by considering image size of 1024×768 pixels and spliced region sizes of 100×100, 200×200 and 512×384.

Method	Spliced Region Size	TPR(%)	TNR(%)	Accuracy(%)
Chen *et al.* [12]	100×100	83.1	84.9	84.8
	200×200	80.7	85.5	85.3
	512×384	84.0	82.6	82.9
Su *et al.* [14]	100×100	84.6	80.3	80.4
	200×200	81.7	85.3	85.0
	512×384	82.8	82.2	82.3
Aizenburg *et al.* [15]	100×100	85.1	83.2	83.3
	200×200	82.8	84.5	84.4
	512×384	87.5	83.1	84.0
Proposed Method	100×100	95.1	94.4	94.5
	200×200	96.8	95.3	95.4
	512×384	95.1	96.6	96.3

We examine the proposed framework in splicing localization by considering different spliced region sizes including 100×100, 200×200 and 512×384 and whole image size of 1024×768 cropped from the original blurred images. We create datasets of tampered images exhibiting blur type inconsistency by splicing the regions extracted from 400 motion blurred images in 400 out-of-focus blurred images, and the regions extracted from 400 out-of-focus blurred images in 400 motion blurred images, at random locations. As such, we have 800 tampered images for each tampered region size. The tampered regions are defined as irregular shapes. It is worth to note that, since in this scenario we consider the natural blurred images, the original image and the spliced region may have different blur degrees. We define two classes including spliced region as the positive class and authentic region as the negative class, which are used to evaluate the splicing localization performance. Table I shows the performances comparison. Our method outperforms the prior works [12], [14], [15] for different spliced region sizes. It can be seen that the performance of our method does not vary much by decreasing the size of tampered region.

Next, we show the effect of resizing on our method and some of the state-of-the-art methods in splicing localization, including JPEG artifacts [2] and CFA artifacts [3] with an example in Fig. 4 (b). Fig. 4 (a) shows an authentic out-of-focus blurred image. By splicing a motion blurred region in image (a), a tampered image is generated with size of 1600×1200, in Fig. 4 (b). After splicing, the tampered image is resized into 1024×768 pixels.

The binary splicing localization maps generated by the methods [2], [3] for the image (b) is shown in Fig. 4 (c)-(d), where the white pixels indicate the possibly tampered areas. To generate such binary maps, the generated probability maps (gray scale maps) using [2], [3] are binarized with the threshold ρ which is chosen in such a way to maximize the average of TPR and TNR on the training set of images. For the generated probability maps using [2], [3], the values between

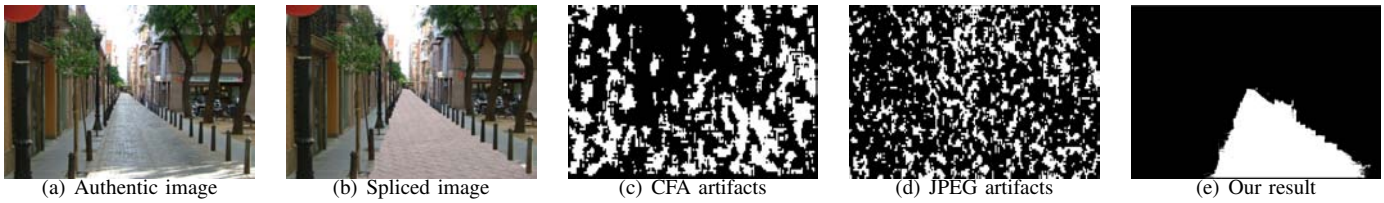

(a) Authentic image (b) Spliced image (c) CFA artifacts (d) JPEG artifacts (e) Our result

Fig. 4: Example of splicing localization in the presence of tampered image resizing. (a) An authentic out-of-focus blurred image. (b) A tampered image generated by splicing a motion blurred region in image (a), followed by resizing. Binary splicing localization maps generated by (c) CFA artifacts [3]; (d) JPEG artifacts [2]; where white pixels indicate high possibility tampered areas. (e) show the results of our method in detection of inconsistent blur types (out-of-focus and motion blur type regions are indicated by white and black regions, respectively) used for splicing localization.

0 and 1 show the probability that splicing occurs. By setting the threshold ρ, the values are classified into the spliced or the authentic regions, indicated by white and black color, respectively. If a value is larger than the threshold, it belongs to the spliced region, or vise versa.

The results reveal that these methods cannot detect the spliced region. Image resizing removes the artifacts used by the CFA [3] and JPEG [2] methods. Therefore, such techniques may not detect the spliced region while our method is more reliable to resizing operation. The result of our method shown in Fig. 4 (e) discriminates the image into out-of-focus and motion blur type regions, indicated in white and black, respectively. Such a discrimination indicates spliced and authentic regions with different blur types.

IV. Conclusions

In this paper, a new method was proposed for splicing localization in a spliced blurred image. After partitioning the image into blocks, the local blur type features are extracted. These local features are incorporated for classification of the image blocks into out-of-focus or motion. Finally, based on the human decision, a multiple blur type image is detected as tampered when the motion blurred region is stationary. In such a case, the different blur types indicate the spliced and authentic regions. The experimental results in the partial blur type detection show that the proposed method classifies the out-of-focus and motion blur types successfully, which outperforms the state-of-the-art methods.

Acknowledgment

This work was carried out at the Rapid-Rich Object Search (ROSE) Lab at the Nanyang Technological University, Singapore. The ROSE Lab is supported by a grant from the Singapore National Research Foundation and administered by the Interactive & Digital Media Programme Office at the Media Development Authority.

References

[1] H. Farid, "Image Forgery Detection," *IEEE Signal Processing Magazine*, 26(2), pp. 16-25, 2009.

[2] T. Bianchi and A. Piva, "Image Forgery Localization via Block-Grained Analysis of JPEG Artifacts," *IEEE Trans. Inf. Forensics Security*, vol. 7, no. 3, pp. 1003-1017, 2012.

[3] P. Ferrara, T Bianchi, A. D. Rosa and A. Piva, "Image Forgery Localization via Fine-Grained Analysis of CFA Artifacts," *IEEE Trans. Inf. Forensics Security*, vol. 7, no. 5, pp. 1566-1577, 2012.

[4] H. Cao and A. C. Kot, "Accurate Detection of Demosaicing Regularity for Digital Image Forensics," *IEEE Trans. Inf. Forensics Security*, vol. 4, no. 4, pp. 899-910, 2009.

[5] Y. F. Hsu and S. F. Chang, "Camera Response Functions for Image Forensics:An Automatic Algorithm for Splicing Detection," *IEEE Trans. Inf. Forensics Security*, vol. 5, no. 4, pp. 816-825, 2010.

[6] M. Chen, J. Fridrich, M. Goljan, and J. Lucas, "Determining Image Origin and Integrity Using Sensor Noise," *IEEE Trans. Inf. Forensics Security*, vol. 3, no. 1, pp. 74-89, 2008.

[7] B. Mahdian and S. Saic, "Blind Authentication Using Periodic Properties of Interpolation," *IEEE Trans. Inf. Forensics Security*, vol. 3, no. 3, pp. 529-538, 2008.

[8] M. C. Stamm, and K. J. R. Liu, "Forensic Detection of Image Manipulation Using Statistical Intrinsic Fingerprints," *IEEE Trans. Inf. Forensics Security*, vol. 5, no. 3, pp. 492-506, 2010.

[9] K. Bahrami, A. C. Kot, and J. Fan, "Splicing Detection in Out-of-Focus Blurred Images," in *Proc. WIFS*, pp. 144-149, 2013.

[10] M. K. Johnson and H. Farid, "Exposing Digital Forgeries in Complex Lighting Environments," *IEEE Trans. Inf. Forensics Security*, vol. 2, no. 3, pp. 450-461, 2007.

[11] H. Yao, S. Wang, Y. Zhao, and X. Zhang, "Detecting Image Forgery Using Perspective Constraints," *IEEE Signal Processing Letters*, vol. 19, no. 7, pp. 123-126, 2012.

[12] X. Chen, J. Yang, Q. Wu, J. Zhao, and X. He, "Directional high-pass filter for blurry image analysis," *Signal Processing:Image Communication*, vol. 27, pp. 760-771, 2012.

[13] R. Liu, Z. Li, and J. Jia, "Image partial blur detection and classification," in *Proc. CVPR*, pp. 1-8, 2008.

[14] B. Su, S. Lu, and C. L. Tan, "Blurred Image Region Detection and Classification," in *ACM Multimedia*, pp. 1397-1400, 2011.

[15] I. Aizenberg, D. V. Paliy, J. M. Zurada, and J. T. Astola, "Blur Identification by Multilayer Neural Network Based on Multivalued Neurons," *IEEE Trans. on Neural Network*, vol. 19, no. 5, pp. 883-898, 2008.

[16] K. Bahrami and A. C. Kot, "Image Tampering Detection by Exposing Blur Type Inconsistency," in *Proc. ICASSP*, pp. 2654-2658, 2014.

[17] K. Sharifi and A. Leon-Garcia, "Estimation of shape parameter for generalized Gaussian distributions in subband decompositions of video," *IEEE Trans. on Circuits and Systems for Video Technology*, vol. 5, no. 1, pp. 52-56, 1995.

[18] A. Levin, Y. Weiss, F. Durand, and W. T. Freeman, "Efficient Marginal Likelihood Optimization in Blind Deconvolution," in *Proc. CVPR*, pp. 2657-2664, 2011.

[19] G. J. McLachlan, "Discriminant Analysis and Statistical Pattern Recognition," *Wiley Interscience*, ISBN 0-471-69115-1. MR 1190469, 2004.

[20] R. Ferzli and L. Karam, "A no-reference objective image sharpness metric based on the notion of just noticeable blur (JNB)," *IEEE Trans. on Image Processing*, vol. 18, no. 4, pp. 717-728, 2009.

[21] A. Levin, D. Lischinski, and Y. Weiss, "A Closed-Form Solution to Natural Image Matting," in *IEEE Trans. on PAMI*, vol. 30, no. 2, pp. 1-15, 2008.